JGR Space Physics

RESEARCH ARTICLE
10.1029/2021JA029987

Key Points:

- We study the longitudinal extent of Pc1 pulsations using 1 year of data obtained at seven ground stations at subauroral latitudes
- The occurrence rates of Pc1 pulsations at subauroral latitudes are highest in the post-noon and lowest in the midnight sector
- The peak of probability distribution of the instantaneous Pc1 longitudinal extent is ∼82.5° with a half maximum at ∼114°

Correspondence to:
K. Shiokawa,
shiokawa@nagoya-u.jp

Citation:
Liu, J., Shiokawa, K., Oyama, S.-I., Otsuka, Y., Jun, C.-W., Nosé, M., et al. (2023). A statistical study of longitudinal extent of Pc1 pulsations using seven PWING ground stations at subauroral latitudes. *Journal of Geophysical Research: Space Physics*, *128*, e2021JA029987. https://doi.org/10.1029/2021JA029987

Received 6 OCT 2021
Accepted 23 DEC 2022

Author Contributions:
Conceptualization: Kazuo Shiokawa
Data curation: Kazuo Shiokawa, Shin-Ichiro Oyama, Yuichi Otsuka, Chae-Woo Jun, Tsutomu Nagatsuma, Kaori Sakaguchi, Akira Kadokura, Mitsunori Ozaki, Martin Connors, Dmitry Baishev, Nozomu Nishitani, Alexey Oinats, Vladimir Kurkin, Tero Raita
Formal analysis: Jie Liu
Funding acquisition: Kazuo Shiokawa, Martin Connors, Dmitry Baishev, Tero Raita
Investigation: Jie Liu
Methodology: Jie Liu, Kazuo Shiokawa, Masahito Nosé
Project Administration: Kazuo Shiokawa, Martin Connors, Dmitry Baishev, Vladimir Kurkin, Tero Raita

A Statistical Study of Longitudinal Extent of Pc1 Pulsations Using Seven PWING Ground Stations at Subauroral Latitudes

Jie Liu[1], Kazuo Shiokawa[1], Shin-Ichiro Oyama[1,2,3], Yuichi Otsuka[1], Chae-Woo Jun[1], Masahito Nosé[1], Tsutomu Nagatsuma[4], Kaori Sakaguchi[4], Akira Kadokura[2,5,6], Mitsunori Ozaki[7], Martin Connors[8], Dmitry Baishev[9], Nozomu Nishitani[1], Alexey Oinats[10], Vladimir Kurkin[10], and Tero Raita[11]

[1]Institute for Space-Earth Environmental Research, Nagoya University, Nagoya, Japan, [2]National Institute of Polar Research, Tokyo, Japan, [3]Space Physics and Astronomy Research Unit, University of Oulu, Oulu, Finland, [4]National Institute of Information and Communications Technology, Koganei, Japan, [5]Polar Environment Data Science Center, Joint Support-Center for Data Science Research, Research Organization of Information and Systems, Tokyo, Japan, [6]The Graduate University for Advanced Studies, Kanagawa, Japan, [7]Kanazawa University, Kanazawa, Japan, [8]Athabasca University, Edmonton, AB, Canada, [9]Yakut Scientific Centre of Siberian Branch of the Russian Academy of Sciences, Yu.G.Shafer Institute of Cosmophysical Research and Aeronomy of Siberian Branch of the Russian Academy of Sciences, Yakutsk, Russia, [10]Institute of Solar-Terrestrial Physics, Siberian Branch of the Russian Academy of Sciences, Irkutsk, Russia, [11]Sodankyla Geophysical Observatory, University of Oulu, Oulu, Finland

Abstract Pc1 geomagnetic pulsations correspond to electromagnetic ion cyclotron (EMIC) waves in the magnetosphere and are excited there with frequencies of 0.2–5 Hz. The instantaneous longitudinal extent of Pc1 waves on the ground has not been estimated yet. In this study, we analyze the Pc1 pulsations observed at seven longitudinally-distributed ground stations at subauroral latitudes at ∼60° magnetic latitude for 1 year from July 2018 to June 2019. The hourly occurrence rates of Pc1 pulsations at all 7 stations have a peak (14%–39.6%) in the post-noon sector and a local minimum (4.1%–8.1%) at midnight. The average frequencies become highest (0.6–1.1 Hz) after midnight and lowest (0.3–0.5 Hz) after noon at all 7 stations. An increasing tendency of total Pc1 occurrence with respect to magnetic latitude was observed. Based on these observations, we obtained a peak of probability distribution of the instantaneous Pc1 longitudinal extent as ∼82.5° with a half maximum at ∼114°, though this probability distribution can be affected by the limitation of the number of the stations. We also made model calculations on the possible longitudinal extent using artificial random Pc1 waves with fixed extents. The comparison of the model results with the observation suggests longitudinal extent of 70°–86° comparable to the peak of probability distribution (∼82.5°). A superposed epoch analysis shows that the longitudinal extent of Pc1 waves tends to increase during recovery phase of geomagnetic storms.

1. Introduction

Pc1 geomagnetic pulsations are commonly observed on the ground at low to high latitudes (e.g., Engebretson et al., 2002; K.-H. Kim et al., 2016; Mann et al., 2014) and are considered as an Ultra-low frequency (ULF) waves in the frequency band of 0.2–5 Hz. The observational discovery of the magnetic pulsations, now called Pc1, is credited to E. Sucksdorff from the Geophysical Observatory at Sodankylä, Finland, and L. Harang from the Auroral Observatory at Tromsø, Norway in 1930s, (e.g., Kangas et al., 1998). Numerous studies have demonstrated that the ground Pc1 waves are generated by electromagnetic ion cyclotron (EMIC) waves near the equatorial plane of the magnetosphere over a wide range of $L \sim 4$–12 (e.g., Anderson et al., 1992a, 1992b; Usanova et al., 2012). Sakaguchi et al. (2013) and Ermakova et al. (2016) reported Pc1 type waves at closer to the Earth at $L \sim 2.5$. The EMIC waves propagate along geomagnetic field lines to be observed as Pc1 pulsations on the ground (e.g., Cornwall, 1965). In addition, Pc1 waves are influenced by the helium gyrofrequency (e.g., Fraser & McPherron, 1982; Young et al., 1981).The EMIC waves are generated because of the anisotropic ($T_\perp > T_\parallel$) distribution of ions providing free energy for instability, where $T_\perp$ and $T_\parallel$ are ion temperatures perpendicular and parallel to the background magnetic field, respectively (e.g., Cornwall, 1965; Yahnina et al., 2000).

Previous statistical studies have illustrated that the occurrence rates of EMIC waves in the magnetosphere increase with increasing L value, that is, increasing radius and higher ground-trace latitude (e.g., Anderson et al., 1992a, 1992b; Usanova et al., 2012). Grison et al. (2021) revealed based on measurements by the Time History of Events and Macroscale Interactions during Substorms (THEMIS) spacecraft that EMIC occurrence

Resources: Kazuo Shiokawa, Shin-Ichiro Oyama, Yuichi Otsuka, Masahito Nosé, Tsutomu Nagatsuma, Kaori Sakaguchi, Akira Kadokura, Mitsunori Ozaki, Martin Connors, Dmitry Baishev, Nozomu Nishitani, Alexey Oinats, Vladimir Kurkin, Tero Raita
Software: Jie Liu, Kazuo Shiokawa, Chae-Woo Jun
Supervision: Kazuo Shiokawa
Validation: Jie Liu, Kazuo Shiokawa, Masahito Nosé
Visualization: Jie Liu, Chae-Woo Jun
Writing – original draft: Jie Liu
Writing – review & editing: Jie Liu, Shin-Ichiro Oyama, Chae-Woo Jun, Tsutomu Nagatsuma

rate is maximum within two Earth radii from the magnetopause and then it linearly decreases with an increasing distance from the magnetopause. Pc1/EMIC waves at subauroral latitudes are considered to be generated near the plasmapause and the occurrence rates at subauroral latitudes usually have a maximum at the post-noon and a minimum after midnight (e.g., Cornwall et al., 1970; Kwon et al., 2020; Usanova et al., 2012). Fraser and Nguyen. (2001) have indicated that drifting energetic ions are considered to cause the EMIC instability. The occurrence peak post-noon is strongly associated with the overlap of energetic ring current ion injection from the plasma sheet with the plasmaspheric bulge and plumes near the dusk sector.

The Pc1 frequencies observed at a ground station at subauroral latitudes are mostly located between the helium and oxygen gyrofrequencies at the conjugate equatorial plasmapause location (e.g., Kangas et al., 1998; K.-H. Kim et al., 2016; Kwon et al., 2020; Sakaguchi et al., 2008). Thus, the variation of wave frequency with local time is attributed to corresponding variations of the gyrofrequencies at the plasmapause.

Through wave-particle interactions, Pc1 waves can contribute to loss of radiation belt electrons and ring current ions into the ionosphere, causing isolated proton auroras (e.g., Kennel & Petschek, 1966; Miyoshi et al., 2008; Ozaki et al., 2016, 2018; Sakaguchi et al., 2015; Thorne & Kennel, 1971; Yahnina et al., 2000). Thus, studying their longitudinal extent is of particular importance for quantitative evaluation of the loss of radiation belt electrons. Engebretson et al. (2015) reported EMIC wave event extending over 12 hr in magnetic local time (MLT) (=180° in longitudes) using multi-point ground and satellite observations. Yahnin et al. (2021) analyzed the longitudinal extent of an event of Pc1/EMIC waves and associated proton precipitation by using multi-spacecraft and multi-station data. Yahnin et al. (2008) have shown that Pc1 are observed within ±2 hr in MLT of the energetic proton precipitation region. There are also several studies of Pc1 waves using latitudinally separated observations (e.g., Afanasyeva, 1978; Kerttula et al., 2001). These latitudinal studies emphasize the significance of the ionospheric conditions for wave observations on the ground, and suggest that the attenuation may occur due to deterioration of the ionospheric Alfvén resonator during the storm main phase.

Using the PWING project (study of dynamic variation of particles and waves in the inner magnetosphere using ground-based network observations) started in 2016 (Shiokawa et al., 2017), for the first time on the global longitudinal scale, longitudinal ground network observations of Pc1 waves have been available at subauroral latitudes. In the present study, we focus on the instantaneous longitudinal extent of Pc1 waves using 1-year data of Pc1 waves obtained at seven ground stations by the PWING project. Through the PWING project, we can statistically analyze the instantaneous longitudinal extent of Pc1 waves at all MLTs. This is a great advantage of the PWING project compared with past statistical studies using single ground stations and/or satellites.

2. Observation

We statistically analyzed simultaneous Pc1 events using the distribution at seven ground stations at subauroral latitudes. The stations are located at Kapuskasing (KAP; 49.39°N, 277.81°E, magnetic latitude (MLAT): 59.0°N), Athabasca (ATH; 54.6°N, 246.36°E, MLAT: 61.5°N), Gakona (GAK; 62.39°N, 214.78°E, MLAT: 63.2°N), Husafell (HUS; 64.67°N, 338.97°E, MLAT: 64.9°N), Zhigansk (ZGN; 66.78°N, 123.37°E, MLAT: 62.23°N), Istok (IST; 70.03°N, 88.01°E, MLAT: 65.9°N), and Oulu (OUL; 65.08°N, 25.90°E, MLAT: 62.13°N). The periods of analyzed data are for 1 year from 1 July 2018–31 May 2019 with an exception of Husafell (HUS) from 1 September 2018–31 August 2019. Figure 1 shows a geographical map of these seven stations. All these stations are located between 59° and 65.9° north magnetic latitudes and roughly form a circle with a similar longitudinal separation. Using data from these stations, we can study the instantaneous longitudinal distribution of Pc1 waves at subauroral latitudes.

Figure 2 shows one example of spectral plots of H-component magnetic field variations at seven stations observed on 13 October 2018. Through the Fast Fourier Transform with a non-overlapping data segment of every 128 s (×64 Hz = 8,192 data points), we calculated power spectral densities (PSDs) and plotted them as dynamic spectra every day in a logarithmic scale of 0.1–32 Hz in vertical axis. Because we do not have absolute value of the magnetic field variations at OUL, we used spectral plots with arbitrary unit for OUL. Clear Pc1 wave events are seen at 6:00–13:00 UT at KAP, and 8:30–12:40 UT and 13:50–17:00 UT at ATH, 2:00–5:00 UT, and 7:00–13:00 UT at GAK, and 2:00–9:00 UT at ZGN, and 3:00–9:30 UT at IST, and 0:30–1:30 UT and 3:30–5:00 UT and 6:00–13:00 UT at OUL, and at 6:00–17:00 UT at HUS.

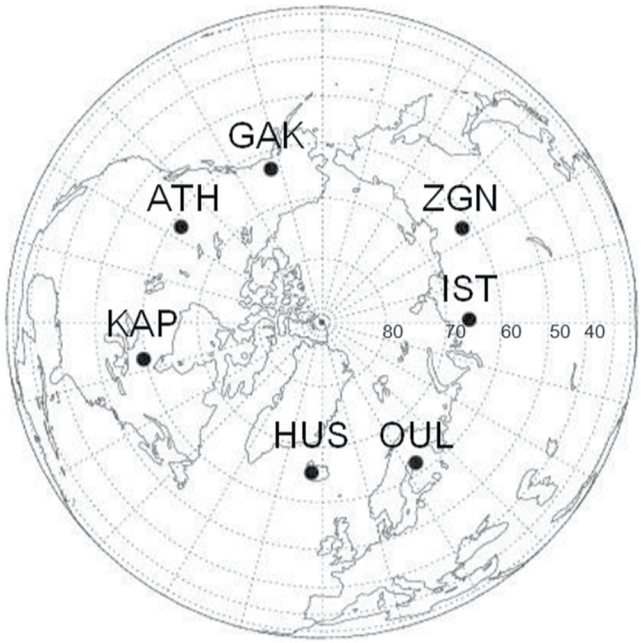

Figure 1. Map of the PWING ground stations in Altitude-Adjusted Corrected Geomagnetic (AACGM) coordinates (epoch: 1 January 2018). All of the stations are located at subauroral latitudes (~60° magnetic latitude) in the northern hemisphere. The stations are Kapuskasing (KAP, 49.39°N, 277.81°E, magnetic latitude (MLAT): 59.0°N), Athabasca (ATH, 54.60°N, 246.36°E, MLAT: 61.5°N), Gakona (GAK, 62.39°N, 214.78°E, MLAT: 63.2°N), Zhigansk (ZGN, 66.78°N, 123.37°E, MLAT: 62.23°N), Istok (IST, 70.03°N, 88.01°E, MLAT: 65.9°N), Oulu (OUL, 65.08°N, 25.90°E, MLAT: 62.13°N), Husafell (HUS, 64.67°N, 338.97°E, MLAT: 64.9°N).

Using these daily dynamic spectral plots, we picked up Pc1 wave events and their oscillation frequencies. The Pc1 wave events are defined through visual inspection of the spectra as (a) band emission at frequencies between 0.2 and 5 Hz with certain bandwidths (which means the emission should disappear below 0.2 Hz), (b) the PSD should be larger than 10^{-6} (nT^2/Hz), and (c) the events are not artificial noise. For ATH, ZGN, GAK, HUS, and KAP, the PSD are shown in unit of (V^2/Hz). Because of the increasing sensitivity with frequencies of the induction magnetometer, the plots in (V^2/Hz) compensate the decreasing tendency of natural wave amplitudes with increasing frequencies, and make it easier to pick up Pc1 pulsations above the instrumental noise level in visual inspection. When we pick up the Pc1 waves, we converted the PSDs to (nT^2/Hz) using sensitivity curves of the magnetometers shown by Shiokawa et al. (2010, 2017). For OUL, we used spectral plots with arbitrary unit, so that we picked up the Pc1 waves by visual inspection without the intensity criterion (b).

Figures 3a and 3b show the total occurrence rate (the blue bars) and the occurrence rate at night (18-06 MLT, the black bars) at each station sorted by magnetic latitudes and longitudes, respectively. The error bars in Figure 3 are estimated by defining the number of Pc1 events m which is shown in the top of the occurrence rate bars in Figure 3. In this case one Pc1 event is defined as a continuous Pc1 event irrespective to its duration. Then, we defined the statistical error of the number of Pc1 events as square root of the number of Pc1 events per station ($\sqrt{m}$). Then the error bars in Figure 3 are estimated by multiplying average duration of the Pc1 events to this statistical error and by dividing it by the total time length of observation.

The total occurrence rates in Figure 3a increase with increasing magnetic latitudes with an exception of OUL. The growth rate of EMIC wave inside the plasmapause is generally lower than that outside the plasmapause, though there is a local enhancement of growth rate near the plasmapause (Cornwall et al., 1970; Horne & Thorne, 1993). This general tendency seems to be consistent with Figure 3a, because the average plasmapause location is at ~60° MLAT (e.g., Carpenter & Anderson, 1992; Moldwin et al., 2002). Min et al. (2012) found the larger occurrence rate of EMIC waves at higher L-shell (higher MLAT), though their results are mainly outside of $L = 4$. In Figure 3b, we do not find clear tendency of longitudinal variation of occurrence rate. The low occurrence rate in OUL may be due to higher noise level at this station compared with other stations, as shown in the spectral examples in Figure 2.

Figure 4 shows the Pc1 wave occurrence rate at seven stations during the available interval. The red curves in these panels show the valid time intervals useable for the data analysis for each MLT hour. Some stations, particularly in ATH and IST, have some data gaps due to instrumental problems, so that the valid time intervals do not reach 1-year value (21,900 min per hour per year). The blue bars indicate the occurrence rates which were derived from the summation of Pc1 event duration times divided by the valid time intervals for each magnetic local-time hour. These seven panels reveal similar tendency that the occurrence rates have the maximum at post-noon local times, except for KAP at 11 MLT, and have the minimum at around midnight in MLT. Additionally, the daytime maximum in the MLT distribution becomes much sharper with increasing latitudes, particularly at IST and HUS and then at GAK. The maximum occurrence rates are highest at IST reaching to 40% and lowest of ~8% at OUL. The minimum occurrence rates are mostly 5%–10% around the midnight.

When selecting the Pc1 waves, we measured the upper and lower boundary frequencies by visual inspection for each Pc1 event. They are defined as maximum and minimum frequencies where the Pc1 power exceeds the criterion of Pc1 intensity (the PSD should be larger than 10^{-6} [nT^2/Hz]) to pick up the Pc1 events. For example, the upper and lower boundary frequencies are 0.2 and 0.8 Hz, respectively at Figure 2g at 1200 UT. Figure 5 indicates upper (red), and lower (blue) boundary frequencies averaged over each magnetic local hour. The black curve shows averages of the upper and lower boundary frequencies. All these curves show a similar tendency for frequency variation, which has the lowest after noon and the highest after midnight, as has been reported in

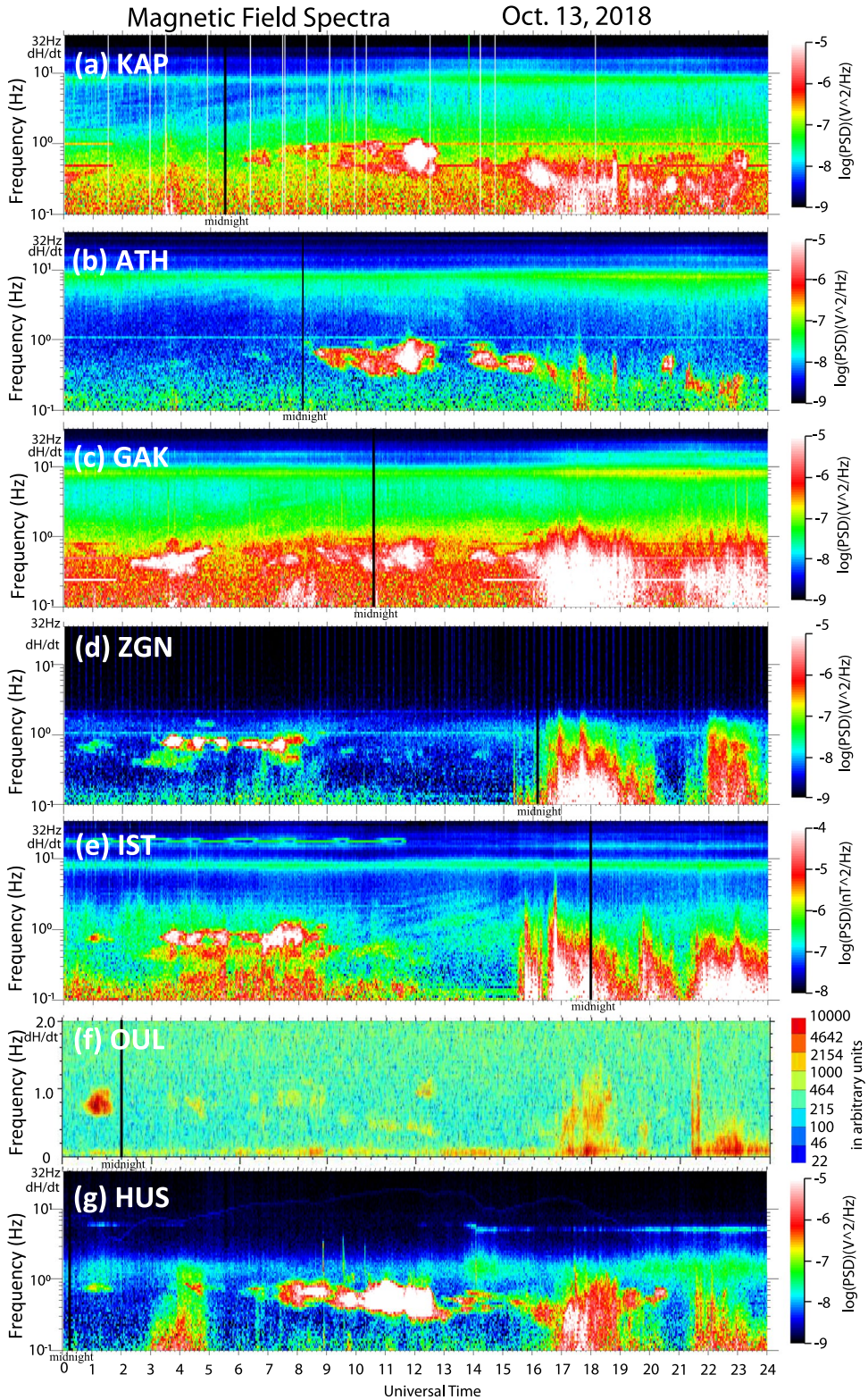

Figure 2. An example of 1-day spectra of H-component magnetic field variations observed (a) Kapuskasing (KAP), (b) Athabasca (ATH), (c) Gakona (GAK), (d) Zhigansk (ZGN), (e) Istok (IST), (f) Oulu (OUL), and (g) Husafell (HUS) on 13 October 2018. Magnetic local midnight is shown by a vertical black line in each panel. The vertical axis is in a logarithmic scale of 0.1–32 Hz. Note that the unit of the power is (V^2/Hz) for most stations except for IST (nT^2/Hz) and OUL (arbitrary unit).

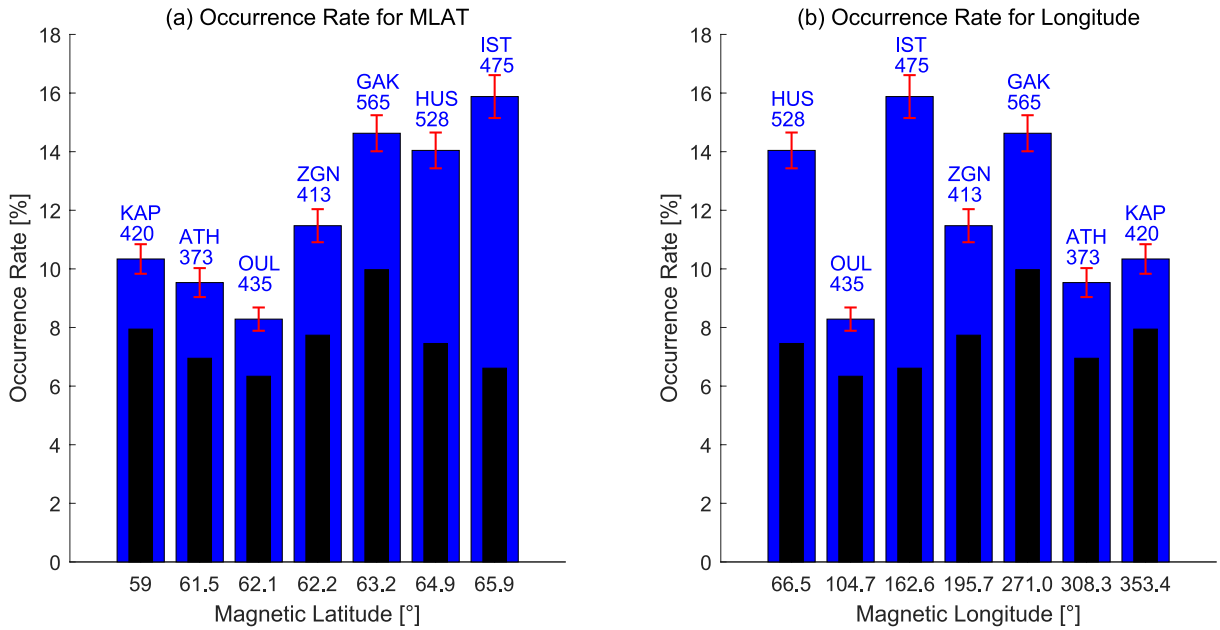

Figure 3. Occurrence rate of Pc1 waves at 7 stations as a function of (a) magnetic latitudes and (b) magnetic longitudes. Numbers shown at the top of the occurrence rate bars are the numbers of Pc1 events. The blue bar indicates the total occurrence rate, while the black bar indicates the occurrence rate at night (18-06 MLT). The error bars are estimated from statistical error of the number of Pc1 events.

previous studies (e.g., Afanasyeva, 1978; Kwon et al., 2020). The lowest and highest average frequencies are 0.3–0.5 and 0.6–1.1 Hz, respectively. The maximum frequencies at lower-latitude stations (e.g., KAP and ATH) tend to be higher compared with those at higher-latitude stations (e.g., HUS and IST).

In order to investigate the typical longitudinal extent of Pc1 waves, we calculated the occurrence rate of Pc1 waves for all single stations and all sets of multiple stations. Figure 6 reveals the occurrence rate for each longitudinal extent. The red stars represent minimum longitudinal extent for Pc1 waves, which are the actual longitudinal separation of stations that observed the Pc1 waves simultaneously. The blue lines indicate the maximum longitudinal extent which is estimated from the observations at multiple stations. For example, for a single station, the minimum longitudinal extent is zero, and the blue bar length is defined as the separation between the neighboring two stations. For multiple stations, the minimum extent (red stars) comes from the separation among the stations where Pc1 waves were detected, and maximum extent (right edge of blue bars) is from the longitudinal separation between the next western and eastern stations. A longitudinal extent shown by blue crosses is estimated to be the mean of the minimum and maximum values (center point of the blue bars).

Figure 6 indicates that the occurrence rate decreases with increasing longitudinal extent. The rate of decrease may indicate the typical longitudinal extent of Pc1 occurrence. The red line indicates fitting to the blue crosses by assuming an exponential function $y = A \times \exp(-Bx)$ with $(A, B) = (27.07, 0.0164)$ through the least square fitting method, where x and y are the longitudinal extent and the occurrence rate, respectively. A (%) corresponds to the occurrence rate for a single station (in case of $x = 0$), and B is the natural logarithm of A divided by inter-station separation, respectively. More detailed explanation of this exponential function is given in the Appendix A of this paper. If the EMIC wave occurrence does not depend on stations, we can expect an exponential decrease of the occurrence rate with increasing longitudinal extent. The average fitting error was ~1.4%.

Figure 7 shows the probability distribution of the longitudinal extent of Pc1 waves obtained by integrating all the occurrence rates shown in Figure 6. The peak of the curve is ~82.5° and a half maximum value at ~114°. The peak value may indicate the most likely occurrence at ~82.5° in the longitudinal extent. We should note that this probability distribution can be affected by the station distributions, that is, the distributions of blue horizontal lines for each (pair) stations in Figure 6.

Figure 8 shows occurrence rates similar to Figure 6 but divided by two Dst index levels. The blue lines and the blue curve are obtained for Pc1 events during Dst index smaller than −15 nT. Only ~2 months of data are

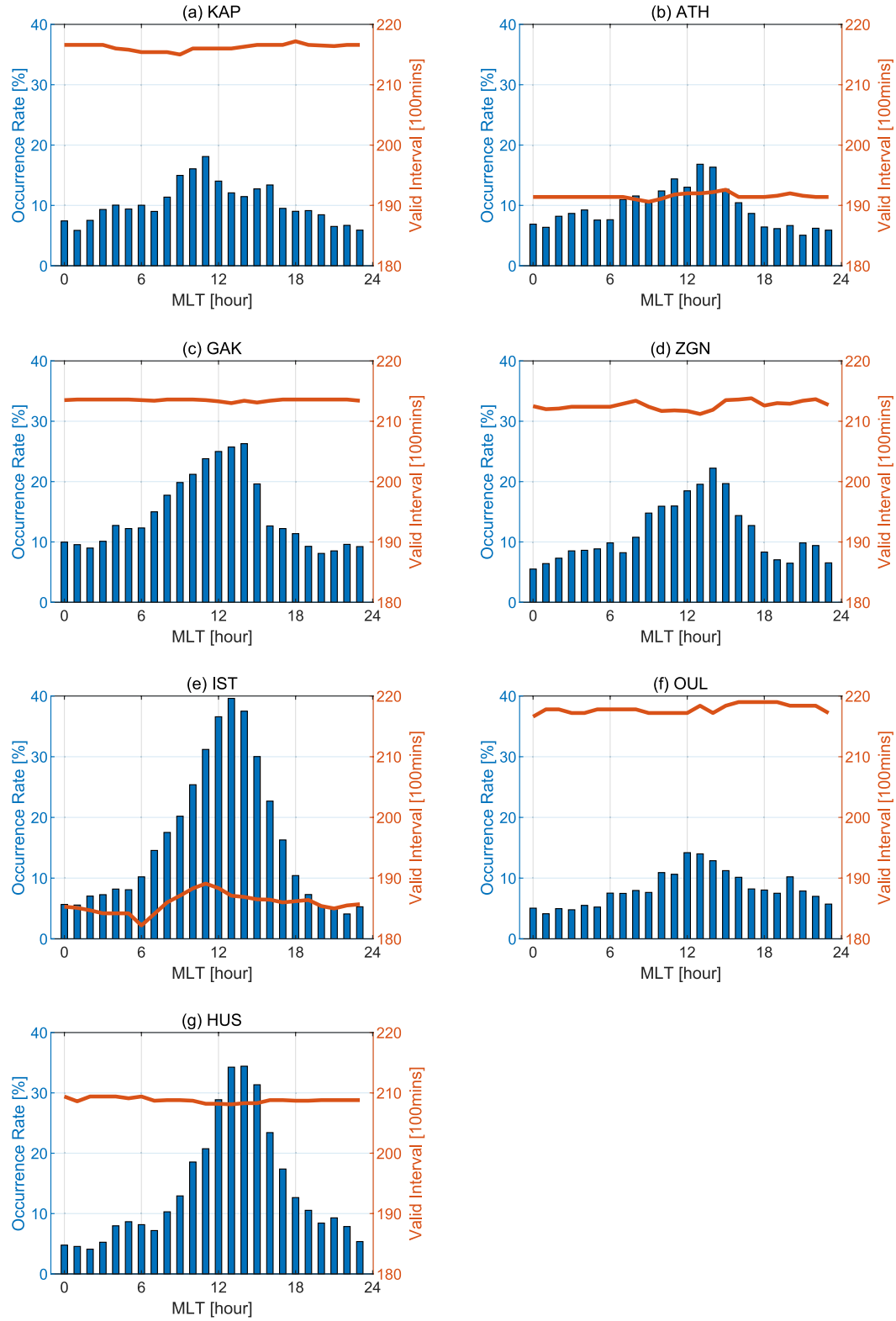

Figure 4. Magnetic local time (MLT) dependence of occurrence rate of the Pc1 waves at (a) Kapuskasing (KAP), (b) Athabasca (ATH), (c) Gakona (GAK), (d) Zhigansk (ZGN), (e) Istok (IST), and (f) Oulu (OUL) from 1 June 2018–31 May 2019 with an exception of (g) Husafell (HUS) from 1 September 2018–31 August 2019. The red curve indicates the valid time interval in unit of 100 min and the blue bars show the occurrence rates for each MLT hour.

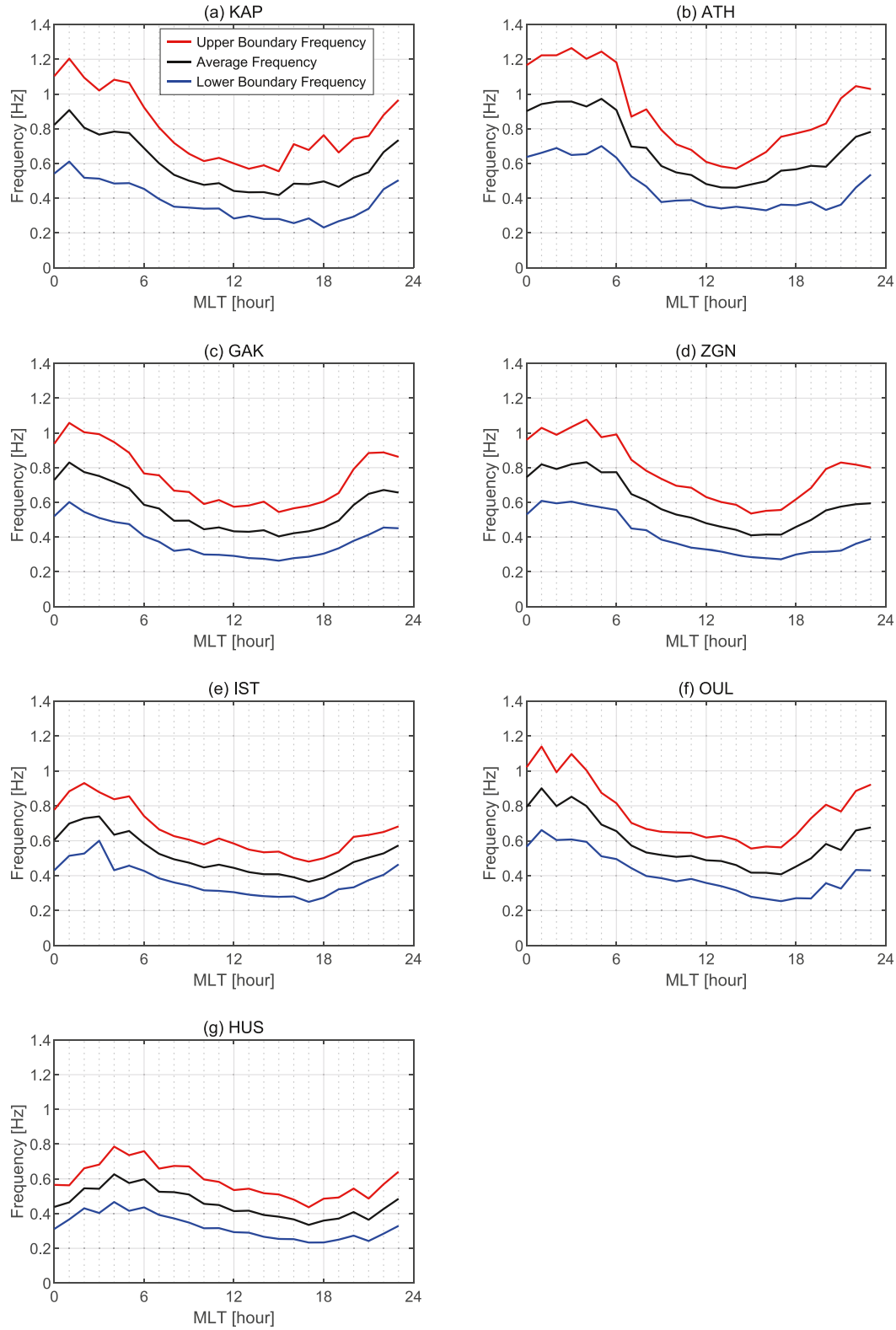

Figure 5. Magnetic local time (MLT) dependence of upper (red) boundary, average (black) and lower (blue) boundary frequencies of Pc1 wave packets for the same data set used in Figure 4 for the 7 stations.

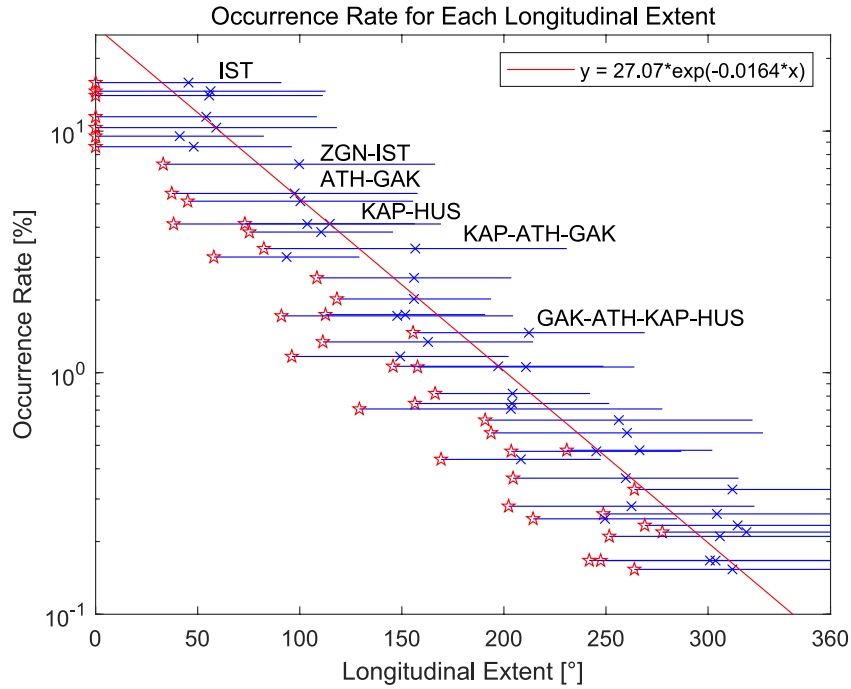

Figure 6. Occurrence rates of Pc1 waves as a function of longitudinal differences between stations. Each line starts from a red star as the actual longitudinal difference of the selected stations (minimum longitudinal extent) and extends to the possible maximum extent which is the longitudinal difference of the neighboring two stations for the selected stations. The red curve shows fitted function of the occurrence rates ($y = A \times \exp(-Bx)$) to the mean values of the possible longitudinal extent indicated by blue crosses.

available for this condition. The green lines and the green curve are for Dst index larger than −15 nT (~10 months of data). We consider these two Dst levels as geomagnetically active period and quiet period, respectively. For most of the longitudinal extents, the occurrence rates in the active period are a little higher than those in the quiet period. However, the difference is not very significant. Due to the limited data sources, we cannot change the threshold Dst value (−15 nT) to further low values to see the difference more clearly.

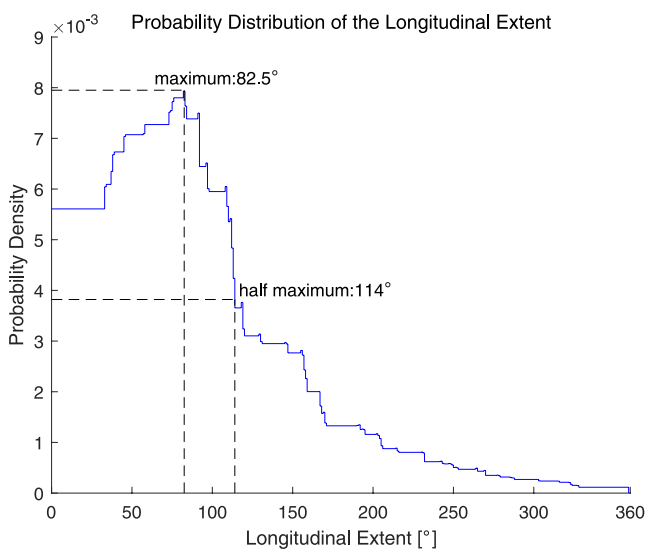

Figure 7. Probability distribution of the longitudinal extent of Pc1 waves obtained by integrating blue bars in Figure 6.

In order to analyze the variation of the longitudinal extent on different geomagnetic activities including storms, we show the relationship between the number of stations with Pc1 per day (the blue curves) and the Dst index (the red curves, daily averages) in Figure 9 for nine months from September 2018 to May 2019. The number of stations with Pc1 per day is defined as the number of stations which observed Pc1 pulsations at least more than 10 min during that day.

In Figure 9, we found a clear tendency that the numbers of stations with Pc1 (blue curves) increase during the recovery phase of geomagnetic storms, for example, in 10–17 September 2018 (the first red box). This suggests the increase of longitudinal extent of Pc1 during the storm recovery phase. For further analysis, we selected seven geomagnetic storms, as indicated by the red boxes in Figure 9, based on visual inspection of daily Dst index. The start of the storm is defined as the sudden decrease of the Dst index, which is the start of the storm main phase. Then the storm recovery phase is defined as the time interval after the Dst minimum. As shown in these red boxes, the number of stations with Pc1 tends to increase during the recovery phase. The end times of the red boxes are taken as the times when this increase of the number of Pc1 stations end.

Figure 10 shows superposed epoch plots of the Dst index and the longitudinal extent of Pc1 waves for the selected seven geomagnetic storms from 3 days

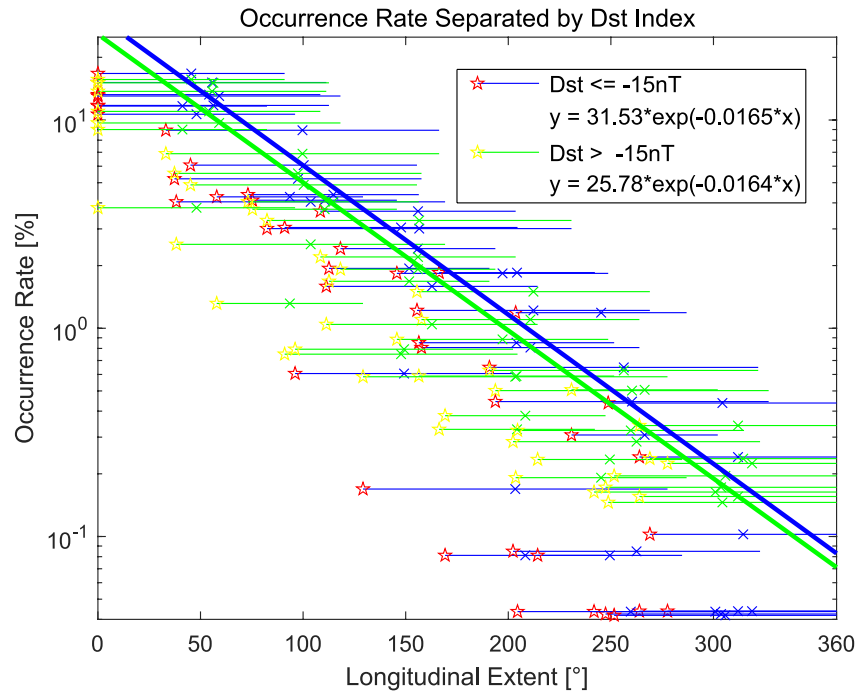

Figure 8. Occurrence rates of Pc1 waves as a function of longitudinal differences between stations (similar to Figure 6) and divided by two Dst ranges. The blue and green indicate active (Dst ≤ -15 nT) and quiet (Dst > -15 nT) intervals, respectively.

before the storm onset (day −3 to day 0) and 10 days after the storm onset (day 0 to day 9). Because the number of stations with Pc1 in Figure 9 may not reflect the actual Pc1 longitudinal extent, we calculated the Pc1 longitudinal extent every hour in the same way to that used to define blue crosses of Figure 6, that is, the average of the extent between the continuous Pc1 stations and the extent of neighboring two stations. If we obtain more than two longitudinal extent values in an hour, we took the maximum value.

In Figure 10, day 0 is mostly the storm main phase where the Pc1 longitudinal extent tends to be small. The Pc1 longitudinal extent start to increase after day 1 when the storm recovery starts. The increase can continue up to 7 days in the recovery phase.

3. Discussion

We have analyzed simultaneous observation of Pc1 waves using seven ground stations at subauroral latitudes, then obtained the occurrence rates of Pc1 waves statistically to estimate the features in longitudinal extent. The present research is the first time the instantaneous longitudinal extent of Pc1 waves at subauroral latitudes has been analyzed statistically, which is important in estimating quantitative loss of relativistic electrons (e.g., Usanova et al., 2014) and subrelativistic electrons (e.g., Blum et al., 2019; Capannolo et al., 2019; Hendry et al., 2019) from the radiation belts. We estimate the maximum occurrence of longitudinal extent of Pc1 waves as ∼82.5° with a half maximum at ∼114° from the probability distribution of the occurrence rate in Figure 7. However, this value can be affected by the limited number of stations (seven) used in the present analysis.

In order to avoid this possible systematic error on the estimation of the typical longitudinal extent, we have made simulations about the occurrence rate of artificial Pc1 waves with fixed longitudinal extent. In the simulation, we assume that the Pc1 waves occur with a fixed longitudinal extent (Φ) throughout 1 year randomly at different longitudes with an average occurrence rate of all the seven stations. In other words, the artificial Pc1 waves occur at various longitudes randomly with the fixed longitudinal extent Φ. The seven ground stations used in the present study make virtual observation of these artificial Pc1 waves and generate the occurrence rate distribution similar to that shown in Figure 6. Because the total occurrence rate increases when increasing the artificial longitudinal extent, we normalized the total occurrence rate of the artificial

Figure 9. The relationship between the number of stations with Pc1 (blue) for each day and the Dst index (red, daily averages) from 1 September 2018 to 31 May 2019. The red boxes indicate the seven geomagnetic storms focused on in this paper and associated increase of the number of Pc1 stations during their recovery phases.

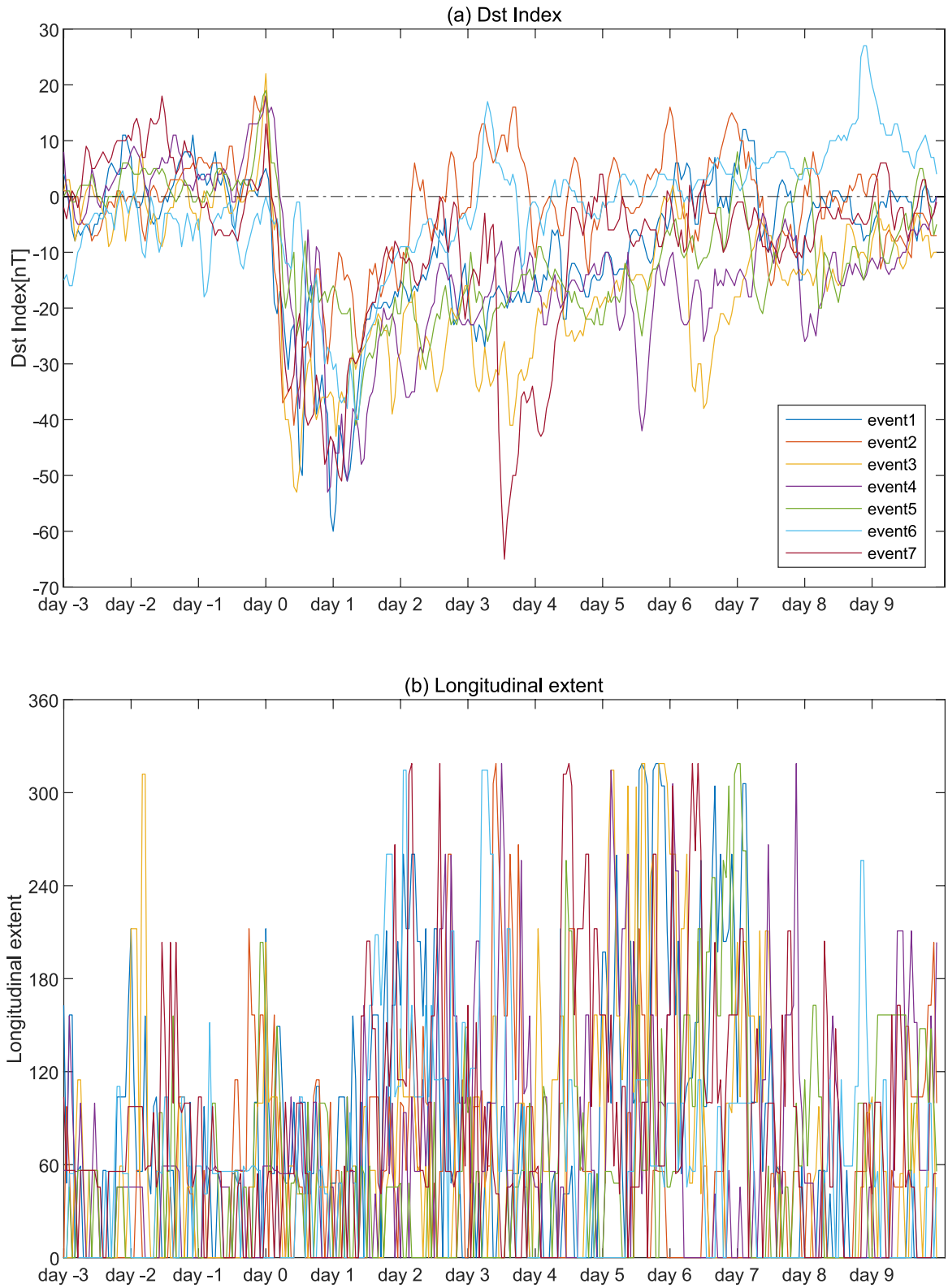

Figure 10. The superposed epoch plots of (a) Dst index and (b) Pc1 longitudinal extent for seven geomagnetic storms with the epoch time of the storm start. The onset times of the events are event 1: 10 UT of 10 September 2018, 2: 21 UT of 21 September 2018, 3: 10 UT of 7 October 2018, 4: 7 UT of 4 November 2018, 5: 11 UT of 19 February 2019, 6: 2 UT of 19 March 2019, and 7: 18 UT of 10 May 2019.

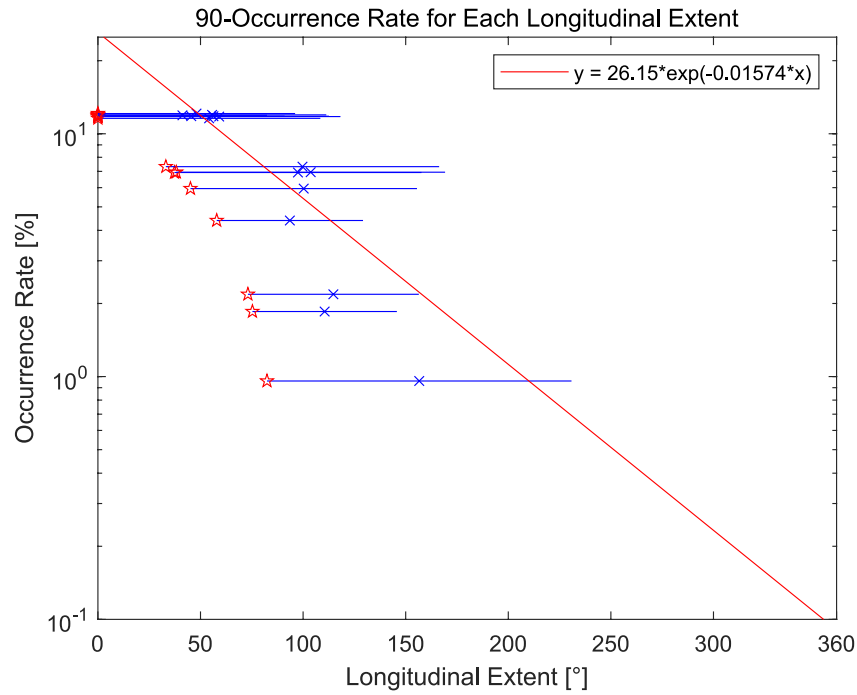

Figure 11. Occurrence rates of Pc1 waves as a function of longitudinal differences between 7 stations, similar to Figure 6, based on simulations of artificial random Pc1 waves with a fixed longitudinal extent $\Phi = 90°$. The red curve shows fitted function of the occurrence rates ($y = A \times \exp(-Bx)$) to the mean values of the possible longitudinal extent indicated by blue crosses.

waves by the total occurrence rate of actual observation. An example of such a virtual observation result is shown in Figure 11 for $\Phi = 90°$. Then we fit an exponential function as shown in the red curve in this virtual observation. It should be noted that because of the assumption of fixed extent, all the occurrence rates at longitudinal separation of more than $\Phi = 90°$ become zero. We did not use the data points with these zero values in the fitting.

Figure 12 shows the fitted exponential functions for different longitudinal extents of artificial Pc1 waves and the curve from the actual observation in Figure 6 (red dotted curve). The order of these lines from bottom to the top is $\Phi = 60°$, 76°, 71°, 80°, 74°, 75°, 85°, actual, 86°, 70°, 87°, 88°, 89°, 90°, 100°, and 120°. The reason why this order does not follow the order of Φ but suddenly jumps back and forth is because of finite number (7) of the stations of observation. The closest curves to the actual observation are those at $\Phi = 85°$ and 86°, but the curves with 75° and 70° are also close. These values are comparable to the maximum occurrence of longitudinal extent of Pc1 waves as ~82.5°.

It is known that the Pc1 waves can propagate horizontally along the ionospheric duct with a typical attenuation rate of 10 dB/1,000 km (e.g., Fujita & Tamao, 1988; Neudegg et al., 2000). In addition to the effects of the ionospheric ducts, Ozaki et al. (2021) reported that ionospheric current variations induced by proton precipitation scattered by EMIC waves in the magnetosphere can be detected as the ground observations of Pc1 waves. Mann et al. (2014) illustrated that the Pc1/EMIC wave emissions can extend ~40° in longitude during propagation from the equatorial plane of the magnetosphere to the ionosphere. The present result of 82.5° should contain these two effects of Pc1/EMIC wave propagation in addition to the longitudinal extent of the EMIC source region in the equatorial magnetosphere.

In Figure 8, we classified the Pc1 occurrence by two Dst levels. The lower Dst curve shows either higher occurrence and/or larger longitudinal extent. By comparing these two curves with simulation of fixed longitudinal extent in Figure 12, we found that the curves at Dst ≤ −15 nT and Dst > −15 nT most fit to the simulation curves with longitudinal extent of 110° and 108°, respectively. This difference is rather small, so we cannot identify a recognizable difference between these two values.

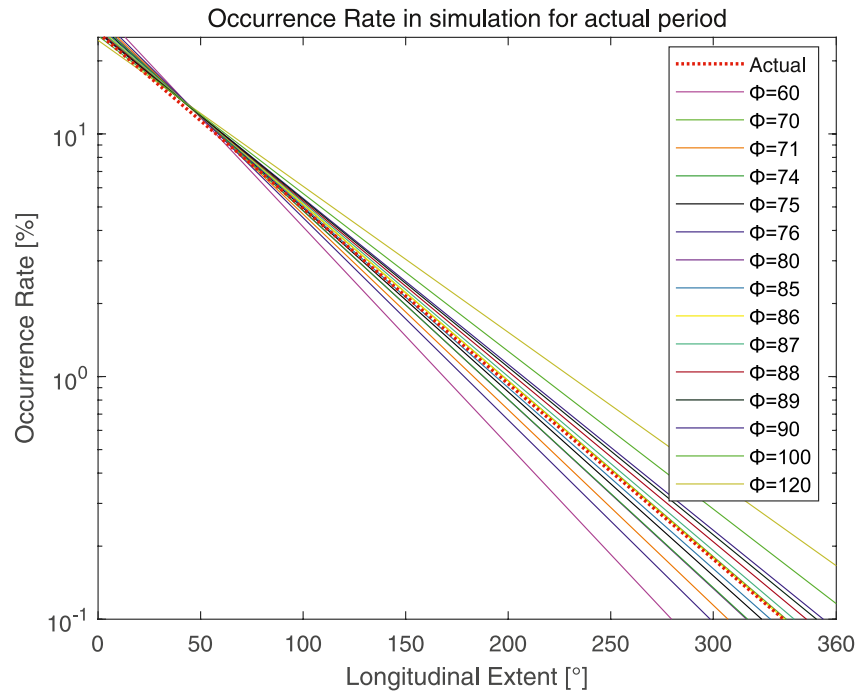

Figure 12. Fitted function of the occurrence rates for simulated artificial random Pc1 waves with various fixed longitudinal extents (Φ). The red dotted curve is fitted from the actual observation taken from Figure 6.

For the total occurrence rate of Pc1 waves, we observed a similar tendency of the occurrence rate with a peak at the post-noon sector among all ground stations except for KAP. The tendency is consistent with several previous studies (e.g., Engebretson et al., 2008; Park et al., 2016; Usanova et al., 2012). Pc1 waves usually seen at the ground are caused by EMIC waves due to westward-drifting ions from the nightside plasma sheet toward the noon. Energetic drifting ions are considered to cause the EMIC instability in the plasmapause region according to the linear growth theory (e.g., Cornwall et al., 1970; Fraser & Nguyen, 2001). Though Horne and Thorne (1993) reported that the growth rate of EMIC wave inside the plasmapause is generally lower than that outside the plasmapause, they also pointed out that the largest amplification of EMIC waves can occur near the plasmapause due to propagation effect in the large density gradient region. Usually, cold plasma extends to higher L-shell in the plasmaspheric bulge in the dusk to post-noon local times (Borovsky et al., 2014). With the penetration of energetic ions into the plasmaspheric bulge, the EMIC waves are expected to occur more frequently at the post-noon sector (e.g., Keika et al., 2013; Usanova et al., 2012). Additionally, there are other possibilities for EMIC wave generation in the dayside. In space, Tetrick et al. (2017) revealed using comprehensive plasma and wave observations by Van Allen Probes that most EMIC waves occurred over an L-range of from −1 to +2 Re relative to the plasmapause. Jun et al. (2019a, 2019b) reported that the post-noon sector near the plasmapause is the major EMIC wave occurrence regions under active geomagnetic conditions in the He^+ band, while H^+ EMIC waves are frequently observed in the morning and noon sectors with dynamic pressure variations. The combination of these EMIC wave distributions can cause the day-night asymmetry of Pc1 occurrence rate at the ground stations near the subauroral regions. The limitation of wave transmission from the magnetosphere to the ground may also contribute to form the local time distribution.

Previous studies indicate that the localized proton enhancement (LPE) is formed by pitch angle scattering of energetic protons by EMIC waves (e.g., Miyoshi et al., 2008; Yahnin & Yahnina, 2007). K.-H. Kim et al. (2016) also investigated the occurrence relation between LPE and Pc1 waves observed in ground stations at subauroral latitude and supported the relationship between LPE and EMIC waves. Through LPE locations, we can estimate the source region of Pc1 waves. Those Pc1 waves observed at subauroral latitude are conjunction with LPE events located in the vicinity of the plasmapause (e.g., Fraser et al., 1989). Some other articles (e.g., Yahnin et al., 2013) also demonstrated that the Pc1 waves at subauroral latitudes have their source region around the plasmapause. When EMIC waves are formed around the plasmapause region, they propagate along the magnetic field lines,

conduct through the ionospheric ducts, and are observed as the Pc1 waves. There are many articles reported that the frequency distribution observed at subauroral latitudes is similar with the gyrofrequencies of helium and oxygen at the plasmapause (e.g., Kangas et al., 1998; K.-H. Kim et al., 2016; Kwon et al., 2020; Sakaguchi et al., 2008), which have a peak after the midnight and a minimum in the afternoon. Our present observation also shows frequency peak after the midnight and minimum in the afternoon for all the 7 stations, which supports the idea that these Pc1/EMIC waves are caused near the plasmapause.

The observations of isolated proton aurora associated with LPE by EMIC wave scattering of protons can show distribution of source region of the EMIC waves at subauroral latitudes (e.g., Nomura et al., 2012; Sakaguchi et al., 2008, 2015; Yahnin et al., 2007). According to these observations, the isolated proton aurora can appear as spot-like features which are often extended in longitudes. This suggests that the overall generation region of EMIC waves can be extended in longitudes, while they have smaller scale structures of stronger and weaker EMIC wave generation within the extended area. Further study on the global distribution of isolated proton aurora with EMIC waves will be important to clarify the longitudinal distribution of EMIC waves.

We obtained an increasing tendency of Pc1 occurrence with respect to magnetic latitudes at the seven ground stations in Figure 3. As we discussed previously, Pc1 waves at subauroral latitudes are considered to be produced near the plasmapause. In the magnetospheric equatorial plane, the occurrence rate of Pc1/EMIC waves is known to increase with the *L*-value from the inner magnetosphere toward the magnetopause (e.g., Anderson et al., 1992a; Usanova et al., 2012). Grison et al. (2021) identified highest wave activity within 1–3 Re (dependent on MLT) from the magnetopause boundary. This may be the reason of the observed increasing tendency of Pc1 occurrence with increasing magnetic latitudes. The EMIC/Pc1 waves propagate from the magnetosphere to the ionosphere along the field lines. These waves are then trapped in the ionospheric duct and propagate latitudinally and longitudinally with attenuation which is related to the electron concentration of ionospheric layer (Kawamura et al., 1981).

In Figures 9 and 10, the number of the stations with Pc1 waves and the Pc1 longitudinal extent tend to increase during storm recovery phase. From ground-based magnetometer observations, it has been reported that significant Pc1 activities are not observed until the recovery phase during geomagnetic storms (e.g., Braysy et al., 1998; Campbell, 1967; J. Kim et al., 2020). Pierrard and Lemaire (2004) illustrated that the plasmaspheric plumes are mostly formed during the geomagnetic storm recovery phase. Engebretson et al. (2008) suggested that the Pc1 waves occurring during the early recovery phase are generated in association with plasmaspheric plumes in the noon-to-dusk sector. On the other hand, Kerttula et al. (2001) proposed the deterioration of ionospheric Alfvén resonator during the storm main phase to explain the attenuation of Pc1 waves during the storm main phase. Engebretson et al. (2008) also revealed that before the recovery phase the propagation of Pc1 waves through the ionospheric waveguide was inhibited severely. Paulson et al. (2017) also saw similar results in space, that is, Pc1 waves occur during magnetically quiet time, particularly during late recovery phase of geomagnetic storms. This may suggest that the depletion of Pc1 during the storm main phase may not be due to an ionospheric effect.

4. Conclusions

We have conducted ground-based simultaneous observation of Pc1 waves using seven stations located at subauroral latitudes for 1 year. We analyzed the occurrence rate of Pc1 waves statistically to estimate the longitudinal extent of the waves. The results of this study are summarized as follows.

1. The hourly occurrence rates have a peak (14%–39.6%) in the post-noon sector and local minimum (4.1%–8.1%) at midnight. The average frequencies of the Pc1 waves become highest (0.6–1.1 Hz) after midnight and lowest (0.3–0.5 Hz) after the noon. These tendencies are same at all the seven stations at subauroral latitudes. This local time dependence of Pc1 frequency suggests that the observed Pc1 waves are generated near the plasmapause. An increasing tendency of total Pc1 occurrence with respect to the magnetic latitudes was observed at the seven stations with exception of OUL.
2. Based on these observations, we statistically estimated the longitudinal extent of the Pc1 waves. The peak of probability distribution of the longitudinal extent is ∼82.5° with a half maximum of ∼114°. We also made simulations of the occurrence rate of random Pc1 waves with fixed longitudinal extents and obtained that the simulated occurrence rate with 70°–86° longitudinal extent, comparable to the peak probability distribution, provides the fit to the actual observation. We cannot find a recognizable difference of longitudinal extent for intervals with Dst > -15 nT and Dst ≤ -15 nT.

3. Using a superposed epoch analysis, we concluded that the longitudinal extent of Pc1 waves increases during the recovery phase of geomagnetic storms.

These results show, for the first time, the longitudinal extent of ground Pc1 waves, which is important to estimate the loss of the radiation belt electrons in the inner magnetosphere through wave-particle interactions quantitatively. However, further study will need to check the PSDs of Pc1 to identify whether the waves are coming from the same resources or not. Such study will distinguish whether the longitudinal extent obtained by multi-point ground stations corresponds to the source distribution in the magnetosphere or more affected by the propagation from the source to the ionosphere and in the ionospheric duct.

Appendix A: Exponential Function of Occurrence Rate

In this appendix, we explain how the exponential function was assumed for fitting to the observed occurrence rates in Figures 6, 8, 11, and 12. Figure A1 shows the schematic figure of the explanation, where x and y are longitudinal separation of stations and occurrence rate, respectively. Assuming that the occurrence rate (α) of Pc1 at single station is identical (e.g., $\alpha = 30\%$) for all the stations, then we can calculate the simultaneous occurrence rate y among the three stations as the value $\alpha \times \alpha \times \alpha = 0.3 \times 0.3 \times 0.3 = 0.027$ (y(Station 1∩Station 2∩Station 3) = α(Station 1) × α(Station 2) × α(Station 3)). Thus, the occurrence rate curve becomes exponential, that is, $y = \alpha^{((x+L)/L)} = \alpha \times \alpha^{(x/L)} = A \times e^{(Bx)}$, where $B = (1/L) \times \ln(\alpha)$ and $A = \alpha$.

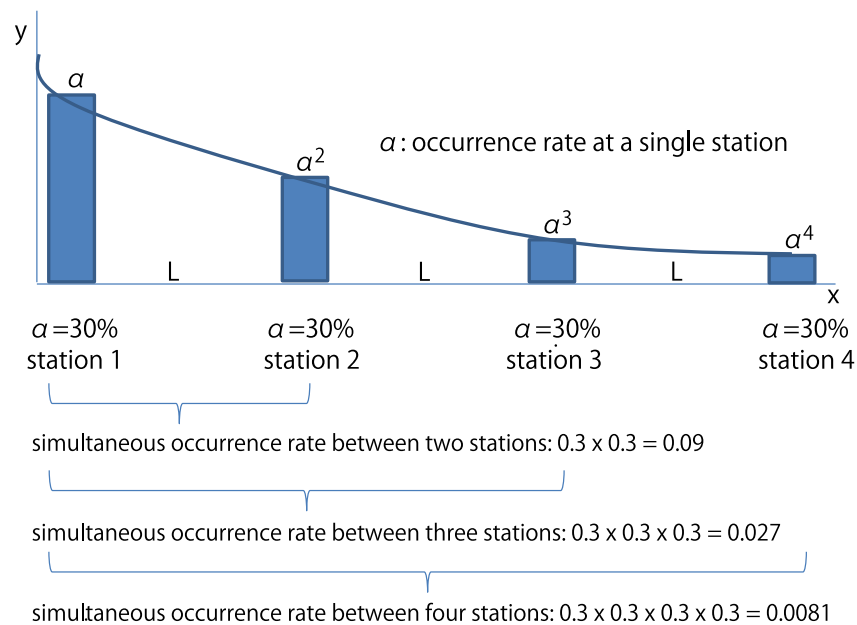

Figure A1. Schematic explanation of exponential function of longitudinal separation versus occurrence rate.

Acknowledgments
This article is based on the PWING project and other grants supported by the Japan Society for the Promotion of Science (JP 15H05747, 16H06286, 21H04518, JPJSBP120194814, JPJSBP120214805, JPJSCCB20210003) and is partially funded by Russian Foundation for Basic Research (21-55-50013; D. B.). Observations at Athabasca are in facilities sponsored by the Canada Foundation for Innovation and at Zhigansk supported by the Ministry of Science and Higher Education of the Russian Federation and the Siberian Branch of the Russian Academy of Sciences (registration number 122011700182-1).

Data Availability Statement

Ground-based data from all the PWING stations can be accessed at the ISEE magnetometer network webpage (http://stdb2.isee.nagoya-u.ac.jp/magne/) and from the ERG Science Center operated by ISAS/JAXA and ISEE/Nagoya University (https://ergsc.isee.nagoya-u.ac.jp/index.shtml.en; Miyoshi et al., 2018). The Dst index data were provided from OMNI Web (http://omniweb.gsfc.nasa.gov/).

References

Afanasyeva, L. T. (1978). Space-time distribution of geomagnetic pulsations and its dependence on the geomagnetic activity. *Acta Geodaetica et Geophysica*, *13*(1–2), 239–271.

Anderson, B. J., Erlandson, R. E., & Zanetti, L. J. (1992a). A statistical study of Pc 1-2 magnetic pulsations in the equatorial magnetosphere: 1. Equatorial occurrence distributions. *Journal of Geophysical Research*, *97*(A3), 3075–3088. https://doi.org/10.1029/91JA02706

Anderson, B. J., Erlandson, R. E., & Zanetti, L. J. (1992b). A statistical study of Pc 1-2 magnetic pulsations in the equatorial magnetosphere: 2. Wave properties. *Journal of Geophysical Research*, *97*(A3), 3089–3101. https://doi.org/10.1029/91JA2697

Blum, L. W., Artemyev, A., Agapitov, O., Mourenas, D., Boardsen, S., & Schiller, Q. (2019). EMIC wave-driven bounce resonance scattering of energetic electrons in the inner magnetosphere. *Journal of Geophysical Research: Space Physics*, *124*(4), 2484–2496. https://doi.org/10.1029/2018JA02642

Borovsky, J. E., Welling, D. T., Thomsen, M. F., & Denton, M. H. (2014). Long-lived plasmaspheric drainage plumes: Where does the plasma come from? *Journal of Geophysical Research: Space Physics*, *119*(8), 6496–6520. https://doi.org/10.1002/2014JA020228

Braysy, T., Mursula, K., & Marklund, G. (1998). Ion cyclotron waves during a great magnetic storm observed by Freja double-probe electric field instrument. *Journal of Geophysical Research*, *103*(A3), 4145–4155. https://doi.org/10.1029/97ja02820

Campbell, W. H. (1967). Low attenuation of hydromagnetic waves in the ionosphere and implied characteristics in the magnetosphere for Pc1 events. *Journal of Geophysical Research*, *72*(13), 3429–3445. https://doi.org/10.1029/jz072i013p03429

Capannolo, L., LiMa, W. Q., Chen, L., Shen, X.-C., Spence, H. E., Sample, J., et al. (2019). Direct observation of subrelativistic electron precipitation potentially driven by EMIC waves. *Geophysical Research Letters*, *46*(22), 12711–12721. https://doi.org/10.1029/2019GL0842

Carpenter, D. L., & Anderson, R. R. (1992). An ISEE/whistler model of equatorial electron density in the magnetosphere. *Journal of Geophysical Research*, *97*(A2), 1097. https://doi.org/10.1029/91ja01548

Cornwall, J. M. (1965). Cyclotron instabilities and electromagnetic emission in the ultra low frequency and very low frequency ranges. *Journal of Geophysical Research*, *70*(1), 61–69. https://doi.org/10.1029/JZ070i001p00061

Cornwall, J. M., Coroniti, F. V., & Thorne, R. M. (1970). Turbulent loss of ring current protons. *Journal of Geophysical Research*, *75*(25), 4699–4709. https://doi.org/10.1029/JA075i025p04699

Engebretson, M. J., Lessard, M. R., Bortnik, J., Green, J. C., Horne, R. B., Detrick, D. L., et al. (2008). Pc1-Pc2 waves and energetic particle precipitation during and after magnetic storms: Superposed epoch analysis and case studies. *Journal of Geophysical Research*, *113*(A1), A01211. https://doi.org/10.1029/2007JA012362

Engebretson, M. J., Peterson, W. K., Posch, J. I., Klatt, M. R., Anderson, B. J., Russell, C. T., et al. (2002). Observations of two types of Pc 1-2 pulsations in the outer dayside magnetosphere. *Journal of Geophysical Research*, *107*(A12), 1451. https://doi.org/10.1029/2001JA000198

Engebretson, M. J., Posch, J. L., Wygant, J. R., Kletzing, C. A., Lessard, M. R., Huang, C.-L., et al. (2015). Van Allen probes, NOAA, GOES, and ground observations of an intense EMIC wave event extending over 12 h in magnetic local time. *Journal of Geophysical Research: Space Physics*, *120*(7), 5465–5488. https://doi.org/10.1002/2015JA021227

Ermakova, E. N., Yahnin, A. G., Yahnina, T. A., Demekhov, A. G., & Kotik, D. S. (2016). Sporadic geomagnetic pulsations at frequencies of up to 15 Hz in the magnetic storm of November 7–14, 2004: Features of the amplitude and polarization spectra and their connection with ion-cyclotron waves in the magnetosphere. *Radiophysics and Quantum Electronics*, *58*(8), 547–560. https://doi.org/10.1007/s11141-016-9628-3

Fraser, B. J., Kemp, W. J., & Webster, D. J. (1989). Ground-satellite study of a Pc1 ion cyclotron wave event. *Journal of Geophysical Research*, *94*(A0), 11855–11863. https://doi.org/10.1029/JA094iA09p11855

Fraser, B. J., & McPherron, R. I. (1982). Pc 1-2 magnetic pulsation spectra and heavy ion effects at synchronous orbit: ATS 6 results. *Journal of Geophysical Research*, *87*(A6), 4560. https://doi.org/10.1029/JA087iA06p04560

Fraser, B. J., & Nguyen, T. S. (2001). Is the plasmapause a preferred source region of electromagnetic ion cyclotron waves in the magnetosphere? *Journal of Atmospheric and Solar-Terrestrial Physics*, *63*(11), 1225–1247. https://doi.org/10.1016/S1364-6826(00)00225-X

Fujita, S., & Tamao, T. (1988). Duct propagation of hydromagnetic waves in the upper ionosphere: 2. Dispersion characteristics and loss mechanisms. *Journal of Geophysical Research*, *93*(A12), 14674–14682. https://doi.org/10.1029/JA093iA12p14674

Grison, B., Santolík, O., Lukačevič, J., & Usanova, M. E. (2021). Occurrence of EMIC waves in the magnetosphere according to their distance to the magnetopause. *Geophysical Research Letters*, *48*(3), e2020GL090921. https://doi.org/10.1029/2020GL090921

Hendry, A. T., Santolík, O., Kletzing, C. A., Rodger, C. J., Shiokawa, K., & Baishev, D. (2019). Multi-instrument observation of nonlinear EMIC-driven electron precipitation at sub-MeV energies. *Geophysical Research Letters*, *46*(13), 7248–7257. https://doi.org/10.1029/2019GL082401

Horne, R. B., & Thorne, R. M. (1993). On the preferred source location for the convective amplification of ion cyclotron waves. *Journal of Geophysical Research*, *98*(A6), 9233. https://doi.org/10.1029/92ja02972

Jun, C.-W., Yue, C., Bortnik, J., Lyons, L. R., Nishimura, Y., Kletzing, C., & Wygant, J. (2019a). EMIC wave properties associated with and without injections in the inner magnetosphere. *Journal of Geophysical Research: Space Physics*, *124*(3), 2029–2045. https://doi.org/10.1029/2018JA026279

Jun, C.-W., Yue, C., Bortnik, J., Lyons, L. R., Nishimura, Y., Kletzing, C., et al. (2019b). A statistical study of EMIC waves associated with and without energetic particle injection from the magnetotail. *Journal of Geophysical Research: Space Physics*, *124*(1), 433–450. https://doi.org/10.1029/2018JA025886

Kangas, J., Guglielmi, A., & Pokhotelov, O. (1998). Morphology and physics of short-period magnetic pulsations. *Space Science Reviews*, *83*(3–4), 435–512. https://doi.org/10.1023/A:1005063911643

Kawamura, M., Kuwashima, M., & Toya, T. (1981). Comparative study of magnetic Pc1 pulsations between low latitudes and high latitudes: Source region and propagation mechanism of the waves deduced from the characteristics of the pulsations at middle and low latitudes. *Memoirs of National Institute of Polar Research: Special Issue*, *18*, 83–100. http://id.nii.ac.jp/1291/00001123/

Keika, K., Takahashi, K., Ukhorskiy, A. Y., & Miyoshi, Y. (2013). Global characteristics of electromagnetic ion cyclotron waves: Occurrence rate and its storm dependence. *Journal of Geophysical Research: Space Physics*, *118*(7), 4135–4150. https://doi.org/10.1002/jgra.50385

Kennel, C. F., & Petschek, H. E. (1966). Limit on stably trapped particle fluxes. *Journal of Geophysical Research*, *71*(1), 1–28. https://doi.org/10.1029/JZ071i001p00001

Kerttula, R., Mursula, K., Pikkarainen, T., & Kangas, J. (2001). Effect of magnetic storm intensity on Pc1 activity at high and mid-latitudes. *Journal of Atmospheric and Solar-Terrestrial Physics*, *63*(5), 503–511. https://doi.org/10.1016/S1364-6826(00)00172-3

Kim, J., Hwang, J., Kim, H., & Yi, Y. (2020). Statistical analysis of Pc1 pulsations observed by a BOH magnetometer. *Journal of Astronomy and Space Sciences*, *37*(1), 19–27. https://doi.org/10.5140/JASS.2020.37.1.19

Kim, K.-H., Shiokawa, K., Mann, I. R., Park, J.-S., Kwon, H.-J., Hyun, K., et al. (2016). Longitudinal frequency variation of long-lasting EMIC Pc1-Pc2 waves localized in the inner magnetosphere. *Geophysical Research Letters*, *43*(3), 1039–1046. https://doi.org/10.1002/2015GL067536

Kwon, J.-W., Kim, K.-H., Jin, H., Kwon, H.-J., Jee, G., Shiokawa, K., & Connors, M. (2020). Statistical study of EMIC Pc1-Pc2 waves observed at subauroral latitudes. *Journal of Atmospheric and Solar-Terrestrial Physics*, *205*, 105292. https://doi.org/10.1016/j.jastp.2020.105292

Mann, I. R., Usanova, M. E., Murphy, K., Robertson, M. T., Milling, D. K., Kale, A., et al. (2014). Spatial localization and ducting of EMIC waves: Van Allen Probes and ground based observations. *Geophysical Research Letters*, *41*(3), 785–792. https://doi.org/10.1002/2013GL058581

Min, K., Lee, J., Keika, K., & Li, W. (2012). Global distribution of EMIC waves derived from THEMIS observations. *Journal of Geophysical Research*, *117*(A5), A05219. https://doi.org/10.1029/2012JA017515

Miyoshi, Y., Hori, T., Shoji, M., Teramoto, M., Chang, T.-F., Segawa, T., et al. (2018). The ERG science center. *Earth Planets and Space*, *70*(1), 1–11. https://doi.org/10.1186/s40623-018-0867-8

Miyoshi, Y., Sakaguchi, K., Shiokawa, K., Evans, D., Albert, J., Connors, M., & Jordanova, V. (2008). Precipitation of radiation belt electrons by EMIC waves, observed from ground and space. *Geophysical Research Letters*, *35*(23), L23101. https://doi.org/10.1029/2008GL035727

Moldwin, M. B., Downward, L., Rassoul, H. K., Amin, R., & Anderson, R. R. (2002). A new model of the location of the plasmapause: CRRES results. *Journal of Geophysical Research*, *107*(A11), 1339. https://doi.org/10.1029/2001JA009211

Neudegg, D. A., Fraser, B. J., Menk, F. W., Waters, C. L., Burns, G. B., & Morris, R. J. (2000). ULF wave attenuation in the high latitude ionospheric waveguide. *Advances in Space Research*, *25*(7/8), 1559–1565. https://doi.org/10.1016/S0273-1177(99)00668-7

Nomura, R., Shiokawa, K., Sakaguchi, K., Otsuka, Y., & Connors, M. (2012). Polarization of Pc1/EMIC waves and related proton auroras observed at subauroral latitudes. *Journal of Geophysical Research*, *117*(A2), A02318. https://doi.org/10.1029/2011JA017241

Ozaki, M., Shiokawa, K., Horne, R. B., Engebretson, M. J., Lessard, M., Ogawa, Y., et al. (2021). Magnetic conjugacy of Pc1 waves and isolated proton precipitation at subauroral latitudes: Importance of ionosphere as intensity modulation region. *Geophysical Research Letters*, *48*(5), e2020GL091384. https://doi.org/10.1029/2020GL091384

Ozaki, M., Shiokawa, K., Miyoshi, Y., Kataoka, R., Connors, M., Inoue, T., et al. (2018). Discovery of 1-Hz range modulation of isolated proton aurora at subauroral latitudes. *Geophysical Research Letters*, *45*(3), 1209–1217. https://doi.org/10.1002/2017GL076486

Ozaki, M., Shiokawa, K., Miyoshi, Y., Kataoka, R., Yagitani, S., Inoue, T., et al. (2016). Fast modulations of pulsating proton aurora related to subpacket structures of Pc1 geomagnetic pulsations at subauroral latitudes. *Geophysical Research Letters*, *43*(15), 7859–7866. https://doi.org/10.1002/2016GL070008

Park, J.-S., Kim, K.-H., Shiokawa, K., Lee, D.-H., Lee, E., Kwon, H.-J., et al. (2016). EMIC waves observed at geosynchronous orbit under quiet geomagnetic conditions (Kp ≤ 1). *Journal of Geophysical Research: Space Physics*, *121*(2), 1377–1390. https://doi.org/10.1002/2015JA021968

Paulson, K. W., Smith, C. W., Lessard, M. R., Torbert, R. B., Kletzing, C. A., & Wygant, J. R. (2017). In situ statistical observations of Pc1pearl pulsations and unstructured EMIC waves by the Van Allen Probes. *Journal of Geophysical Research: Space Physics*, *122*(1), 105–119. https://doi.org/10.1002/2016JA02316

Pierrard, V., & Lemaire, J. F. (2004). Development of shoulders and plumes in the frame of the interchange instability mechanism for plasmapause formation. *Geophysical Research Letters*, *31*(5), L05809. https://doi.org/10.1029/2003GL018919

Sakaguchi, K., Kasahara, Y., Shoji, M., Omura, Y., Miyoshi, Y., Nagatsuma, T., et al. (2013). Akebono observations of EMIC waves in the slot region of the radiation belts. *Geophysical Research Letters*, *40*(21), 5587–5591. https://doi.org/10.1002/2013GL058258

Sakaguchi, K., Shiokawa, K., Miyoshi, Y., & Connors, M. (2015). Isolated proton auroras and Pc1/EMIC waves at subauroral latitudes. In Y. Zhang & L. J. Paxton (Eds.), *Auroral dynamics and space weather*. https://doi.org/10.1002/9781118978719.ch5

Sakaguchi, K., Shiokawa, K., Miyoshi, Y., Otsuka, Y., Ogawa, T., Asamura, K., & Connors, M. (2008). Simultaneous appearance of isolated auroral arcs and Pc 1 geomagnetic pulsations at subauroral latitudes. *Journal of Geophysical Research*, *113*(A5), A05201. https://doi.org/10.1029/2007JA012888

Shiokawa, K., Katoh, Y., Hamaguchi, Y., Yamamoto, Y., Adachi, T., Ozaki, M., et al. (2017). Ground-based instruments of the PWING project to investigate dynamics of the inner magnetosphere at subauroral latitudes as a part of the ERG-ground coordinated observation network. *Earth Planets and Space*, *69*(1), 160. https://doi.org/10.1186/s40623-017-0745-9

Shiokawa, K., Nomura, R., Sakaguchi, K., Otsuka, Y., Hamaguchi, Y., Satoh, M., et al. (2010). The STEL induction magnetometer network for observation of high-frequency geomagnetic pulsations. *Earth Planets and Space*, *62*(6), 517–524. https://doi.org/10.5047/eps.2010.05.003

Tetrick, S. S., Engebretson, M. J., Posch, J. L., Olson, C. N., Smith, C. W., Denton, R. E., et al. (2017). Location of intense electromagnetic ion cyclotron (EMIC) wave events relative to the plasmapause: Van Allen Probes observations. *Journal of Geophysical Research: Space Physics*, *122*(4), 4064–4088. https://doi.org/10.1002/2016JA023392

Thorne, R. A., & Kennel, C. F. (1971). Relativistic electron precipitation during magnetic storm main phase. *Journal of Geophysical Research*, *76*(19), 4446–4453. https://doi.org/10.1029/JA076i019p04446

Usanova, M. E., Drozdov, A., Orlova, K., Mann, I. R., Shprits, Y., Robertson, M. T., et al. (2014). Effect of EMIC waves on relativistic and ultrarelativistic electron populations: Ground-based and Van Allen Probes observations. *Geophysical Research Letters*, *41*(5), 1375–1381. https://doi.org/10.1002/2013GL059024

Usanova, M. E., Mann, I. R., Bortnik, J., Shao, L., & Angelopoulos, V. (2012). THEMIS observations of electromagnetic ion cyclotron wave occurrence: Dependence on AE, SYMH, and solar wind dynamic pressure. *Journal of Geophysical Research*, *117*(A10), A10218. https://doi.org/10.1029/2012JA018049

Yahnin, A. G., Popova, T. A., Demekhov, A. G., Lubchich, A. A., Matsuoka, A., Asamura, K., et al. (2021). Evening side EMIC waves and related proton precipitation induced by a substorm. *Journal of Geophysical Research: Space Physics*, *126*(7), e2020JA029091. https://doi.org/10.1029/2020JA029091

Yahnin, A. G., & Yahnina, T. A. (2007). Energetic proton precipitation related to ion-cyclotron waves. *Journal of Atmospheric and Terrestrial Physics*, *69*(14), 1690–1706. https://doi.org/10.1016/j.jastp.2007.02.010

Yahnin, A. G., Yahnina, T. A., Frey, H., & Pierrard, V. (2013). Sub-oval proton aurora spots: Mapping relatively to the plasmapause. *Journal of Atmospheric and Terrestrial Physics*, *99*, 61–66. https://doi.org/10.1016/j.jastp.2012.09.018

Yahnin, A. G., Yahnina, T. A., & Frey, H. U. (2007). Subauroral proton spots visualize the Pc1 source. *Journal of Geophysical Research*, *112*(A10), A10223. https://doi.org/10.1029/2007JA012501

Yahnin, A. G., Yahnina, T. A., & Frey, H. U. (2008). Identification of sources of Pc1 geomagnetic pulsations on the basis of proton aurora observations. *Cosmic Research*, *46*(4), 344–347. https://doi.org/10.1134/S0010952508040084

Yahnina, T. A., Yahnin, A. G., Kangas, J., & Manninen, J. (2000). Proton precipitation related to Pc1 pulsations. *Geophysical Research Letters*, *27*(21), 3575–3578. https://doi.org/10.1029/2000GL003763

Young, D. T., Perraut, S., Roux, A., De Villedary, C., Gendrin, R., Korth, A., et al. (1981). Wave-particle interactions near Ω_{He+} observed on GEOS 1 and 2 1. Propagation of ion cyclotron waves in He+– rich plasma. *Journal of Geophysical Research*, *86*(A8), 6755. https://doi.org/10.1029/JA086iA08p06755